# Retrievals for the atmospheric chemistry experiment Fourier-transform spectrometer

Chris D. Boone, Ray Nassar, Kaley A. Walker, Yves Rochon, Sean D. McLeod, Curtis P. Rinsland, and Peter F. Bernath

SCISAT-1, also known as the Atmospheric Chemistry Experiment, is a satellite mission for remote sensing of the Earth's atmosphere, launched on 12 August 2003. The primary instrument on the satellite is a 0.02 $cm^{-1}$ resolution Fourier-transform spectrometer operating in the mid-IR (750–4400 $cm^{-1}$). We describe the approach developed for the retrieval of atmospheric temperature and pressure from the troposphere to the lower thermosphere as well as the strategy for the retrievals of volume-mixing ratio profiles of atmospheric species. © 2005 Optical Society of America

*OCIS codes:* 010.1280, 280.0280, 300.6340.

## 1. Introduction

SCISAT-1, the first in a planned series of small science satellites developed under the auspices of the Canadian Space Agency, features a fully tilt and shear compensated Fourier-transform spectrometer (FTS) with high resolution (±25 cm maximum optical path difference) and broad spectral coverage in the mid-IR (750–4400 $cm^{-1}$). As summarized by Bernath *et al.*,[1] the primary goals of the of the SCISAT-1 Atmospheric Chemistry Experiment (ACE) mission are (1) to understand the chemical and the dynamic processes that control the distribution of ozone in the stratosphere and upper troposphere, particularly in the Arctic; (2) to explore the relationship between atmospheric chemistry and climate change; (3) to study the effects of biomass burning in the free troposphere; and (4) to measure aerosols and clouds to reduce uncertainties in their effects on global energy balance.

Use of a high-resolution FTS to monitor the limb of the atmosphere was pioneered by the Atmospheric Trace Molecule Spectroscopy (ATMOS) experiment,[2] a mission that flew four times on the NASA Space Shuttle (1985, 1991, 1992, and 1993) and recorded a remarkable series of high-resolution (±50 cm optical path difference) solar occultation spectra. Currently there are two other high-resolution FTSs in orbit: the tropospheric emission spectrometer[3] (TES) on NASA's Aura satellite and the Michelson interferometer for passive atmospheric sounding[4] (MIPAS) on the European Space Agency's ENVISAT satellite. The TES and MIPAS, however, monitor the thermal emission of the atmospheric limb (in the nadir mode as well for TES). Limb emission spectroscopy offers improved global coverage (day and night) at the expense of the signal-to-noise ratio (SNR) and/or spectral resolution compared with solar occultation.

The SCISAT-1 FTS (called the ACE-FTS) measures concentration profiles for more than 20 atmospheric constituents with altitude coverage extending from cloud tops to 150 km, taking advantage of the high spectral resolution of the FTS and the sensitivity of the solar occultation technique. The nominal duration of the mission is 2 years. Besides the ACE-FTS, the SCISAT-1 payload also includes a dual optical spectrograph known as the measurement of aerosol extinction in the stratosphere and troposphere retrieved by occultation (MAESTRO), designed to cover the 285–1030 nm spectral region with a vertical resolution of ~1 km, providing measurements primarily of ozone, nitrogen dioxide, and aerosol/cloud extinction. The small instrument package on the satellite also features a pair of 128 × 128 pixel complementary metal-oxide semiconductor (CMOS) detector arrays to provide solar images at 525 ± 1 and 1020 ± 1 nm, closely matching the wavelengths of the

C. D. Boone (e-mail, cboone@acebox.uwaterloo.ca), R. Nassar, K. A. Walker, S. D. McLeod, and P. F. Bernath are with the University of Waterloo, Department of Chemistry, 200 University Avenue West, Waterloo, Ontario N2L 3G1, Canada. C. P. Rinsland is with NASA Langley Research Center, Atmospheric Sciences Division, Hampton, Virginia 23681-2199. Y. Rochon is with Meteorological Service of Canada, Environment Canada, Toronto, Ontario, Canada.

Received 22 March 2005; revised manuscript received 26 July 2005; accepted 8 August 2005.

0003-6935/05/337218-14$15.00/0

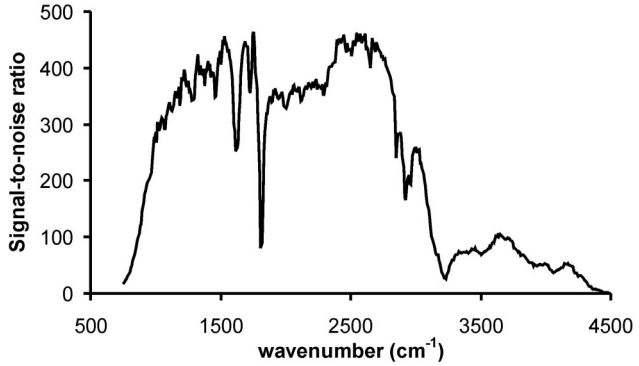


Fig. 1. Signal-to-noise ratio as a function of wavenumber for the ACE-FTS as determined from transmittance spectra collected in January 2005. The sharp drop near 1810 $cm^{-1}$ is in the overlap region between the instrument's two detectors. The drop near 3250 $cm^{-1}$ is due to ice contamination.

Stratospheric Aerosol and Gas Experiment II (SAGE II).[5]

In the present paper we describe the spectral analysis software and the inversion procedures used to derive the vertical profiles of temperatures and of the volume mixing ratios of molecular species from the ACE IR solar absorption spectra.

## 2. ACE-FTS Measurements

The ACE-FTS instrument is described in more detail by Soucy *et al.*,[6] but a summary of instrument parameters relevant to the retrievals is given here. Sun pointing is achieved with a suntracker that points to the center of radiance by balancing signal outputs on a quadrant detector operating at 1.55 μm. The ACE-FTS uses two photovoltaic detectors: HgCdTe (750–1810 $cm^{-1}$) and InSb (1810–4400 $cm^{-1}$). At full spectral resolution the scan time is 2 s. The altitude spacing of the FTS measurements, controlled by the scan time and the orbit of the satellite, is typically 3–4 km. It varies with the beta angle, the angle between the satellite velocity vector and a vector from the Earth to the Sun, where a beta angle of zero features the sun setting (or rising) exactly perpendicular to the Earth horizon. The altitude spacing ranges from 2 km for long occultations with high beta (~55°) to 6 km for occultations with beta angle zero. Note that the field of view of the instrument is circular with a diameter of 1.25 mrad, which gives a maximum altitude resolution between 3 and 4 km for a satellite ~2700 km from the tangent point.

Both ACE-FTS detectors are cooled to less than 100 K (typically 80–90 K) by a passive radiator pointing toward deep space. An example of the SNR performance for the instrument is shown in Fig. 1. The drop-off in SNR at the lowest wavenumbers is related to the HgCdTe detector performance. The reduced SNR performance at higher wavenumbers is the result of beam-splitter transmission problems. The dip in the SNR near 1810 $cm^{-1}$ is in the overlap region between the two detectors. The dip centered near 3250 $cm^{-1}$ is caused by ice absorption. The ice arises mainly from water outgassed from the satellite's multilayer insulation blankets. Periodic decontamination of an intermediate stage window of the detector/cooler package with onboard heaters removes the ice and improves the SNR performance. Every few months a full decontamination of the detectors is performed, heating all stages of the cooler rather than just the intermediate stage. The rate of ice buildup slows gradually as the mission progresses.

Both ACE-FTS detectors are photovoltaic, an improvement over the ATMOS mission in terms of detector linearity, which is important for the study of aerosols and clouds.[7] Spectra measured by the ACE-FTS require no corrections for detector nonlinearity.

The solar occultation approach features an inherent self-calibrating advantage. Measurements with the ACE-FTS pointed toward deep space are used to correct for self-emission of the instrument. High Sun measurements (i.e., measurements with tangent altitudes of 160–225 km and containing no atmospheric spectral signatures) are used to remove solar spectral features and the effects of instrumental response. Calibration spectra are collected for each ACE occultation.

## 3. ACE-FTS Retrievals

An accurate knowledge of atmospheric pressure and temperature as a function of altitude is essential for retrieval of volume mixing ratio (VMR) profiles. For the altitude range of ACE-FTS measurements (5–150 km) it is not possible to obtain sufficiently accurate meteorological data from *a priori* information. Pressure and temperature profiles are therefore determined from the ACE-FTS spectra. For ACE-FTS processing, $CO_2$ is analyzed to determine pressure and temperature, a standard strategy for IR remote-sensing instruments.[8,9]

A crucial aspect of the pressure and temperature retrieval process is pointing knowledge. No information from sensors onboard the satellite (other than a clock) is used in the computation of tangent altitudes. The future processing of ACE-FTS data will employ satellite sensor data to derive pointing, but the current approach treats tangent altitudes as unknown parameters in the pressure/temperature (P/T) retrievals.

Rather than fitting the entire spectrum, we analyze microwindows, small portions of the spectrum (generally 0.3–1 $cm^{-1}$ wide) that contain spectral features from a molecule of interest with minimal spectral interference from other molecules. For some molecules it is not possible to find a comprehensive set of microwindows free from significant interferences. Thus the VMR retrieval software allows for retrieval of as many as six molecules simultaneously. All retrievals employ a modified global fit approach,[10] in which all parameters are determined simultaneously with the Levenberg–Marquardt[11] nonlinear least-squares method.

The ACE-FTS processing software has undergone

three revisions. The original data release (Version 1.0) was intended for testing the stability of the software and for early validation efforts. Version 2.0 improved on the P/T retrieval approach, but a change in interpolation strategy made the VMR retrievals more susceptible to unphysical oscillations. Version 2.1 addressed the problem of unphysical oscillations and improved other aspects of the retrievals but was used only to analyze a subset of the ACE-FTS data. The current processing version is 2.2 and is similar to Version 2.1 but with improvements in high-altitude temperatures (for the mesopause and above). Version 2.2 is used to analyze the entire ACE-FTS data set. The differences between the retrieval approaches for the different versions are described in detail below.

### A. Atmospheric Model

Calculating spectra (for least-squares fitting) must invoke a parameterized model of the Earth's atmosphere. For the effective sea level as a function of latitude we adopt the ellipsoid model from the World Geodetic System 1984 (WGS 84).[12] The acceleration due to gravity at sea level $g_0$ as a function of latitude is derived from the WGS 84 model. In order to keep calculations analytical (including derivatives for the least-squares process), the variation in acceleration due to gravity with altitude $z$ is approximated as a linear function of $z$, accurate to within a tenth of a percent in the altitude range of interest.

By virtue of its long atmospheric lifetime, $CO_2$ is well mixed and has a nearly constant VMR over much of the middle atmosphere. At high altitudes, photodissociation and diffusion reduce the VMR. The altitude above which the $CO_2$ VMR drops off varies with season and location: typically 80–90 km (Ref. 13) but extending below 60 km during the polar winter at extreme latitudes.[14] For Versions 2.1 and 2.2 of the ACE-FTS processing, $CO_2$ VMR is assumed to be constant as high as 75 km for latitudes below 60° and as high as 65 km for latitudes greater than 60°. Previous versions assumed a constant $CO_2$ VMR as high as 70 km for all latitudes.

To account for the increase in $CO_2$ VMR as a function of time, we adopt the equation used by the Halogen Occultation Experiment[15] (HALOE):

$$CO_2 \text{ VMR (ppm)} = 326.909 + 1.50155(t - t_0),$$

$$t_0 = 1 \text{ January } 1977,$$

in which $t - t_0$ is time in years. We assume a bulge for $CO_2$ VMR in the troposphere, ~5.5 ppm greater than the stratospheric value. No provisions are made for variations with location or season. Note that, because the $CO_2$ VMR below ~70 km is fixed during P/T retrievals, errors in the assumed profile will unavoidably translate into errors in the VMR retrievals for other molecules.

#### 1. Forward Model

The calculation grid adopted for the ACE-FTS analysis is divided into 150 layers of 1 km thickness. Each layer is assumed to have a constant temperature, pressure, and VMR for a given molecule with no consideration of horizontal gradients within a layer. Diurnal corrections are not currently applied, although diurnal effects are likely to be significant for photosensitive molecules such as $NO_2$.

The raw wavenumber spacing for the ACE-FTS spectra is 0.02 $cm^{-1}$. To achieve accurate results for the narrow lines found at high tangent altitudes, forward model calculations are performed on a much finer grid, with a wavenumber spacing reduced by a factor of 16.

The forward model for ACE-FTS is the same radiative-transfer model used for ATMOS with some notable exceptions: (1) ACE-FTS forward model calculations employ the HITRAN 2004 line list and cross sections.[16] (2) Partition functions for the ACE-FTS forward model are calculated from the total internal partition sums (TIPS) approach.[17] (3) The Voigt lineshape function is calculated from the Humlicek algorithm[18,19] rather than from a lookup table. (4) No apodization is used for the ACE-FTS instrumental line shape (ILS). (5) The ILS for the ACE-FTS requires an empirical adjustment to account for self-apodization effects beyond the normal field of view contribution.

#### 2. ACE-FTS Instrumental Line-Shape Model

The finite extent of the FTS scan gives rise to a truncated interferogram. This induces a ringing effect for sharp features in the FTS spectrum. The finite scan time can be represented by a windowing function in interferogram space, a simple rectangular (boxcar) function of the optical path difference or time. Additional instrumental effects are modeled by adjusting this windowing function, which is otherwise known as the modulation function. The ILS is defined as the Fourier transform of the modulation function. For an ideal instrument the ILS would be a pure sinc function ($\sin x/x$), the Fourier transform of a rectangular function.

The FTS spectrum $S_{FTS}$ is calculated by convolving the input monochromatic spectrum $S_{input}$ with the ILS:

$$S_{FTS}(\tilde{\nu}) = \int S_{input}(\tilde{\nu}')\text{ILS}(\tilde{\nu} - \tilde{\nu}')\text{d}\tilde{\nu}', \qquad (1)$$

where $\tilde{\nu}$ are wavenumber units ($cm^{-1}$). In principle the integral extends from minus to plus infinity, but in practice a truncated version of the integral is calculated on a discrete grid. The number of points used in the ILS [in other words the extent of the integral in Eq. (1)] is a trade-off between accuracy and calculation speed.

The modulation function *MF* as a function of the optical path difference ($x$ in centimeters) for a given wavenumber $\tilde{\nu}$ is calculated as

Table 1. ACE-FTS ILS Empirical Parameters from Eq. (3)

| Coefficient | HgCdTe Detector Region | InSb Detector Region |
|---|---|---|
| $a(\tilde{\nu})^a$ | $-5.61698 \times 10^{-4} - \Delta\tilde{\nu} \times 1.65872 \times 10^{-6}$ | $2.0205 \times 10^{-3} - \Delta\tilde{\nu} \times 2.6965 \times 10^{-7}$ |
| $b(\tilde{\nu})$ | $7.427198 \times 10^{-5} + \Delta\tilde{\nu} \times 1.81971 \times 10^{-7}$ | $-1.51007 \times 10^{-4} + \Delta\tilde{\nu} \times 7.594546 \times 10^{-8}$ |
| $c(\tilde{\nu})$ | $-1.35606 \times 10^{-6} - \Delta\tilde{\nu} \times 4.52998 \times 10^{-9}$ | $3.97629 \times 10^{-6} - \Delta\tilde{\nu} \times 1.848666 \times 10^{-9}$ |

[a] $\Delta\tilde{\nu}$ is $\tilde{\nu} - 2400\ \mathrm{cm}^{-1}$.

$$MF(\tilde{\nu}, x) = \mathrm{rect}(x)\eta(\tilde{\nu}, x)\frac{\sin(\frac{1}{2}\pi r^2\tilde{\nu}x)}{\frac{1}{2}\pi r^2\tilde{\nu}x}, \qquad (2)$$

where $r$ is the radius in radians of the circular field of view.

The first term in Eq. (2), rect($x$), is the rectangular function arising from the finite scan. For the ACE-FTS it will be 1 for $x$ between $\pm 25$ cm and 0 otherwise. The third term in Eq. (2), the sinc function, represents the effect of a finite field of view.[20]

The second term in Eq. (2), $\eta$, is an empirical function used to account for the additional sources of self-apodization. For the ACE-FTS a relatively simple peaked function was selected:

$$\eta(\tilde{\nu}, x) = \exp\left[-a(\tilde{\nu})x^2 - b(\tilde{\nu})|x|^3 - c(\tilde{\nu})x^4\right], \qquad (3)$$

where coefficients $a$, $b$, and $c$ are adjustable parameters. The coefficients vary slowly as a function of wavenumber, and so a linear variation was deemed sufficiently accurate.

The coefficients in Eq. (3) were determined by a nonlinear least-squares fitting of lines spanning from 800 to 4000 $\mathrm{cm}^{-1}$ with separate results for the two detector regions. The lines used were restricted to higher altitudes, such that the underlying spectral features were narrow compared with the ILS. The results are in Table 1. The ILS is stable, there is no indication of significant changes as a function of time. There is also no significant asymmetry evident in the ILS.

It is common practice to suppress ringing in the spectrum by apodizing the modulation function,[21] artificially reducing the abruptness of the interferogram clipping by forcing the windowing function to tend smoothly to zero at the extremes. In a preliminary study for ACE-FTS retrievals by using ATMOS data,[22] VMR profiles retrieved with and without apodization agreed within the fitting errors, but apodization induced greater (likely unphysical) variability in the profiles. Propagating forward the effect of apodization on the covariance matrix of the observations[23] (rather than using a diagonal matrix) may reduce this variability, but we chose to avoid explicit apodization.

When analyzing microwindows without the use of apodization, it is important to consider the finite extent of the ILS. Enough points must be included in the convolution to capture all significant far wing contributions from lines outside the microwindow. The typical extent of the ACE-FTS ILS is $\sim 0.5\ \mathrm{cm}^{-1}$. (All points within $\pm 0.5\ \mathrm{cm}^{-1}$ are used in the convolution with the ILS.) For $CO_2$ greater than 60 km in the pressure/temperature retrievals the extent of the ILS is increased to $1.6\ \mathrm{cm}^{-1}$ for Versions 2.1 and 2.2 of the processing software.

In a separate paper the justifications for (and consequences of) not using apodization for ACE-FTS analysis are discussed, but note that the unexpected self-apodization could almost be considered a benefit, suppressing sidelobes without the need to manipulate the measured spectrum, as one would with artificial apodization.

*3. Interpolation onto the 1 km Altitude Grid*

In the retrieval process, physical quantities (pressure, temperature, and/or VMR) are determined on a nonuniform altitude grid, i.e., at the tangent altitudes. However, forward model calculations occur on a fixed 1 km grid. Piecewise quadratic interpolation is used to cast information from the retrieval grid onto the 1 km grid. For temperature or the VMR the interpolation onto the 1 km grid uses three measurements (at tangent heights $z_1$, $z_2$, and $z_3$) and takes the following form:

$$X(z) = \frac{(z-z_2)(z-z_3)}{(z_1-z_2)(z_1-z_3)}X_1 + \frac{(z-z_1)(z-z_3)}{(z_2-z_1)(z_2-z_3)}X_2 + \frac{(z-z_1)(z-z_2)}{(z_3-z_1)(z_3-z_2)}X_3, \qquad (4)$$

where $X$ = VMR or 1/T and $z$ is the altitude at the center of a given layer.

The P/T retrievals for the ACE FTS assume that the atmosphere is in a hydrostatic equilibrium, i.e., that at a given altitude the upward force due to the density gradient balances the weight of overhanging air. Interpolation onto the 1 km grid for pressure therefore takes hydrostatic equilibrium into account. The equation for hydrostatic equilibrium can be written as

$$\frac{\mathrm{d}P(z)}{\mathrm{d}z} = -g(z)\rho(z) = -\frac{g(z)m_a(z)P(z)}{kT(z)}, \qquad (5)$$

where $g$ is acceleration due to gravity, $\rho$ is density, $m_a$ is the average molecular mass, and $k$ is the Boltzmann constant. Note that the ideal gas law was used to write density as a function of pressure and temperature.

The average molecular mass $m_a$ in Eq. (5) poses a difficulty. It is constant below $\sim 85$ km, but above

that it decreases with increasing altitude. The variation in $m_a$ with altitude is estimated by using the NRL-MSISE-00 software (commonly referred to as MSIS) from the U.S. Naval Research Laboratories.[24] For a given time and geographic location, MSIS generates temperature and density from an empirical model, where the inputs to the model are the daily solar flux at a wavelength of 10.7 cm and geomagnetic parameters. MSIS generates number densities for eight atomic and molecular constituents. At altitudes greater than 80 km this information is fitted to express the average molecular mass as a fifth-order polynomial in altitude.

When an approximate linear form for $g(z)$ and the expression for $1/T(z)$ from Eq. (4) are used, Eq. (5) becomes

$$P(z') = P_3 \exp\left\{ -\frac{g_0}{k} \int_{z_3}^{z'} m_a(z)\left(1 - \frac{2z}{R_e}\right) \times \left[ \frac{(z - z_2)(z - z_3)}{(z_1 - z_2)(z_1 - z_3)} \frac{1}{T_1} + \frac{(z - z_1)(z - z_3)}{(z_2 - z_1)(z_2 - z_3)} \frac{1}{T_2} + \frac{(z - z_1)(z - z_2)}{(z_3 - z_1)(z_3 - z_2)} \frac{1}{T_3} \right] dz \right\}, \quad (6)$$

$$m_a(z) = \begin{cases} 28.94 \text{ atomic mass units}, & z < 80 \text{ km} \\ a + bz + cz^2 + dz^3 + ez^4 + fz^5, & z \geq 80 \text{ km} \end{cases},$$

where $R_e$ is the effective radius of the Earth at the given latitude (determined from the WGS 84 model). As long as $P$ and $T$ at the measurement tangent heights obey hydrostatic equilibrium, the interpolation expression in Eq. (6) ensures that the physical model on the 1 km grid also obeys hydrostatic equilibrium.

When a fixed calculation grid is employed, the tangent layer must be considered as a special case. For a solar ray traveling through the tangent layer the values for pressure, temperature, and the VMR at the center of the layer do not represent well the average values of the quantities experienced by the solar ray during transit (unless the tangent height is at the bottom of the layer). Several approaches are available to address this problem. For ACE-FTS processing the absorption coefficient in the tangent layer is taken as a weighted average of the value calculated for the tangent layer and the value calculated for the layer directly above. The weighting factor is determined by the distance from the tangent height to the top of the layer. This approach assumes a roughly linear variation of the absorption coefficient as a function of altitude over the span of 1 km.

### B. Pressure/Temperature Retrievals

As mentioned above a prerequisite for accurate VMR retrievals is to determine accurate $P$ and $T$ profiles by analysis of $CO_2$. The P/T retrievals separate naturally into two distinct altitude regions, high altitude and low altitude, and so the two regions are treated independently.

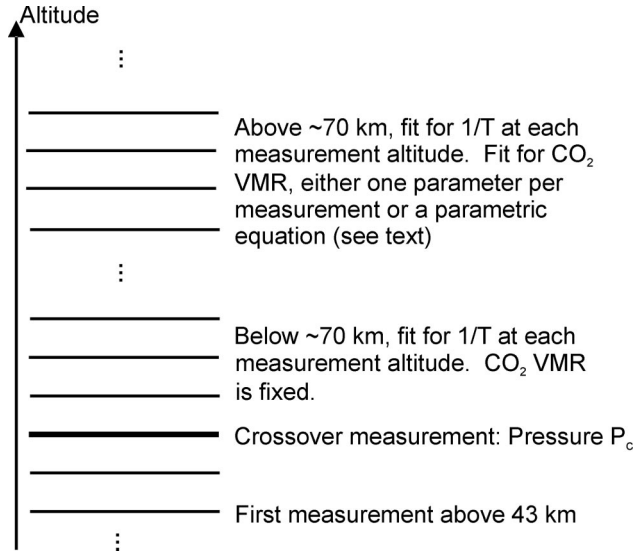


Fig. 2. High-altitude portion of the P/T retrieval. Analysis extends from the crossover measurement as far as 115 km (Versions 1.0 and 2.0) or 120 km (Versions 2.1 and 2.2). The only parameter for pressure in this region $P_c$ can either be fixed or serve as a fitting parameter. All pressures are calculated from this single parameter by using hydrostatic equilibrium.

At high altitudes the $CO_2$ VMR cannot be readily determined from *a priori* information. However, there are no features (such as significant refraction or optically thick clouds) that affect instrument pointing in this altitude region, and so tangent heights can be reliably calculated from geometry, from knowledge of the relative positions of the Sun, Earth, and satellite. This requires an accurate characterization of the satellite's orbit and an accurate measure of time. Note that there is a known systematic problem with ACE-FTS measurement times. The absolute values for time stamps are not considered reliable, but differences between time stamps are presumed accurate. As a consequence only the spacing between calculated tangent heights is reliable. Absolute tangent heights in this altitude region are determined through the registration procedure described below.

At low altitudes the situation is reversed: $CO_2$ VMR is assumed known and can be reliably fixed, but tangent heights cannot be calculated from geometry. The boundary between low altitude and high altitude is taken to be 43 km.

#### 1. *High Altitudes*

Figure 2 depicts the high-altitude portion of the P/T retrieval. For reasons that become clear below, the crossover measurement is taken as the third measurement greater than 43 km and is typically around 50 km. An analysis extends from the crossover to

as high as 115 km for Versions 1.0 and 2.0, while Versions 2.1 and 2.2 extend as high as 120 km.

For each measurement there are four potential variables ($P$, $T$, VMR, and tangent height $z$) that must be either fixed or fitted. The data support at most two unknowns per measurement for least-squares fitting (two because there is information from both the absolute and relative intensities of the lines).

In the high-altitude region the set of fitting parameters includes $1/T$ for each measurement. However, the region requires only one parameter for pressure: $P_c$, the pressure at the crossover measurement. From this single parameter (and values for tangent height and temperature at each measurement) the pressures for all other measurements in this region are calculated from the expression in Eq. (6), integrating upward from the crossover measurement.

In the altitude range between the crossover and ~70 km the $CO_2$ VMR is fixed. Above this the $CO_2$ VMR is fitted. For Versions 1.0 and 2.0 the fitting parameters were simply $CO_2$ VMR at each measurement. For these software versions the $CO_2$ VMR for the highest analyzed measurement must be fixed or the process is underconstrained (i.e., there are too many unknown parameters). We predetermined $CO_2$ VMR for the highest analyzed measurement by using a least-squares fitting with $P$ and $T$ fixed to MSIS values.

With the expectation that $CO_2$ VMR at high altitudes would not exhibit sharp structure, Versions 2.1 and 2.2 use an empirical function to reduce the number of fitting parameters:

$$CO_2\ \mathrm{VMR}(z) = \frac{\mathrm{VMR}_{\mathrm{strat}} + a(z - z_0) + b(z - z_0)^2 + c(z - z_0)^3}{1 + d(z - z_0) + e(z - z_0)^2}, \quad (7)$$

where $\mathrm{VMR}_{\mathrm{strat}}$ is the assumed stratospheric value for $CO_2$ and $z_0$ is taken as the highest tangent height for which $CO_2$ VMR is assumed constant. As mentioned above, for Versions 2.1 and 2.2 the $CO_2$ VMR is assumed constant as high as 75 km for latitudes less than 60° and 65 km for latitudes greater than 60°. A Padé approximant form (the ratio of two polynomials) is used in Eq. (7) because it requires fewer parameters than a straight polynomial, and the extrapolation beyond the fitting region is better.

*2. Low Altitudes*

Figure 3 shows the configuration for the low-altitude portion of the P/T retrievals. Analysis in this altitude region extends from the measurement below the crossover to as low as 12 km. This analysis can proceed only if the pressure at the crossover $P_c$ is known (e.g., from an analysis of the high-altitude portion).

As before the four potential variables ($z$, $P$, $T$, and VMR) need to be established for each measurement. The $CO_2$ VMR is fixed to its assumed profile. The value of $1/T$ at each measurement serves as a fitting parameter. For Version 1.0, $P$ at each measurement (excluding the measurement below the crossover) represents a fitting parameter. For Versions 2.0, 2.1, and 2.2 the measurements below ~25 km use an empirical expression to determine pressure in order to reduce the number of fitting parameters.

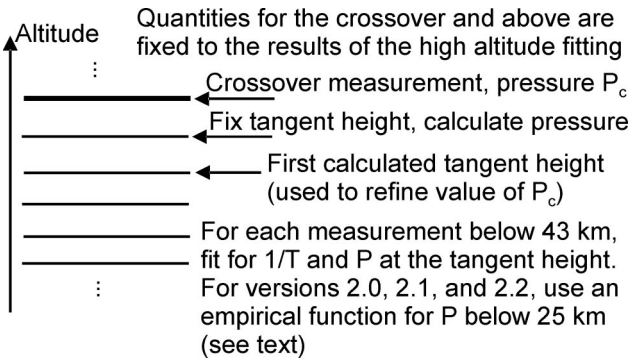


Fig. 3. Low-altitude portion of the P/T retrieval. The high-altitude portion of the retrieval must be performed in a previous step. Analysis extends from the measurement below the crossover to as low as 12 km. Tangent heights in this region are calculated from hydrostatic equilibrium.

The empirical expression chosen was inspired by the work of Rinsland *et al.*,[25] where it was noted that the baseline in the region of $N_2$ + $CO_2$ continua obeyed a consistent function of density for a diverse set of atmospheric conditions. For ACE-FTS processing we consider the ratio of the baseline at 2442.6 and 2502 $\mathrm{cm}^{-1}$ (denote this ratio as $R_b$). We are not concerned here with the details of the function and do not rely on theoretical information for the relationship. Our only concern is that tangent density be a smooth function of $R_b$ as verified by a study of the Version 1.0 results. The density at the tangent height $\rho_{\mathrm{tangent}}$ is written as

$$\rho_{\mathrm{tangent}} = \exp\left(\frac{a + bR_b + cR_b^2}{1 + \mathrm{d}R_b}\right) \mathrm{molecules/cm}^3, \quad (8)$$

and tangent pressure is calculated from the ideal gas law. Thus for Versions 2.0, 2.1, and 2.2 the four coefficients in Eq. (8) serve as the fitting parameters for pressure between 12 and 25 km.

Note that for pressure the measurement below the crossover is a special case required for the fitting process in this region to be adequately constrained. For this measurement the tangent height is fixed to its calculated value, and pressure is calculated from Eq. (6), integrating downward from the crossover. This leaves $1/T$ as the only fitted parameter for the measurement.

Tangent heights in this altitude region are expressed as a function of pressure and temperature through the constraint of hydrostatic equilibrium. Starting from the relation for hydrostatic equilibrium in Eq. (5), the integral from the crossover measurement (altitude $z_c$) to the measurement below the crossover (altitude $z_{c+1}$) is

$$\int_{z_c}^{z_{c+1}} \frac{dP}{P} = -\frac{g_0 m_a}{k} \int_{z_c}^{z_{c+1}} \left(1 - \frac{2z}{R_e}\right) \times \left[ \frac{(z - z_{c+1})(z - z_{c+2})}{(z_c - z_{c+1})(z_c - z_{c+2})} \frac{1}{T_c} + \frac{(z - z_c)(z - z_{c+2})}{(z_{c+1} - z_c)(z_{c+1} - z_{c+2})} \frac{1}{T_{c+1}} + \frac{(z - z_c)(z - z_{c+1})}{(z_{c+2} - z_c)(z_{c+2} - z_{c+1})} \frac{1}{T_{c+2}} \right] dz. \quad (9)$$

Note that the average molecular mass $m_a$ is constant in this altitude region. The integral on the left-hand side is evaluated analytically. The integrand of the right-hand side of Eq. (9) is a cubic function of $z$. Thus Simpson's rule for evaluating the integral represents an exact solution. Making use of Simpson's rule and rearranging yield

$$\frac{6k}{g_0 m_a} \ln\left(\frac{P_{c+1}}{P_c}\right) = \alpha \left[ \frac{2}{T_c} + \frac{2}{T_{c+1}} + \frac{\beta - \alpha}{\beta} \frac{1}{T_c} + \frac{\beta}{\beta - \alpha} \frac{1}{T_{c+1}} - \frac{\alpha^2}{\beta(\beta - \alpha)} \frac{1}{T_{c+2}} \right] - \frac{2\alpha}{R_e} \left[ \left(2z_c - \frac{\alpha}{2}\right) \frac{1}{T_c} + \left(2z_c - \frac{3\alpha}{2}\right) \frac{1}{T_{c+1}} \right] - \frac{2\alpha}{R_e} \left(z_c - \frac{\alpha}{2}\right) \times \left[ \frac{\beta - \alpha}{\beta} \frac{1}{T_c} + \frac{\beta}{\beta - \alpha} \frac{1}{T_{c+1}} - \frac{\alpha^2}{\beta(\beta - \alpha)} \frac{1}{T_{c+2}} \right], \quad (10)$$

where $\alpha \equiv (z_c - z_{c+1})$ and $\beta \equiv (z_c - z_{c+2})$. Note that $\beta$ is the only unknown in Eq. (10) because $z_c$ and $z_{c+1}$ are both known. It is possible to determine $\beta$ (hence $z_{c+2}$) with the solution of a cubic equation. However, the pressure at the target measurement $P_{c+2}$ does not factor into Eq. (10). This leads to stability problems in the retrieval. Thus we consider also the integration from $z_c$ to $z_{c+2}$:

$$\frac{6k}{g_0 m_a} \ln\left(\frac{P_{c+2}}{P_c}\right) = \beta \left[ \frac{2}{T_c} + \frac{2}{T_{c+2}} + \frac{\alpha - \beta}{\alpha} \frac{1}{T_c} - \frac{\beta^2}{\alpha(\alpha - \beta)} \frac{1}{T_{c+1}} + \frac{\alpha}{\alpha - \beta} \frac{1}{T_{c+2}} \right] - \frac{2\beta}{R_e} \left[ \left(2z_c - \frac{\beta}{2}\right) \frac{1}{T_c} + \left(2z_c - \frac{3\beta}{2}\right) \times \frac{1}{T_{c+2}} \right] - \frac{2\beta}{R_e} \left(z_c - \frac{\beta}{2}\right) \left[ \frac{\alpha - \beta}{\alpha} \frac{1}{T_c} - \frac{\beta^2}{\alpha(\alpha - \beta)} \frac{1}{T_{c+1}} + \frac{\alpha}{a - \beta} \frac{1}{T_{c+2}} \right]. \quad (11)$$

Equation (11) contains $P_{c+2}$, but the solution for $\beta$ would involve solving a quartic equation. The two simultaneous equations can be combined to cancel the term in $\beta^4$, leading to a cubic expression of $\beta$ more appropriate than the one in Eq. (10):

$$\frac{1}{R_e}\left(\frac{1}{T_c} - \frac{1}{T_{c+1}}\right)\beta^3 + \left[\left(\frac{1}{T_c} - \frac{1}{T_{c+1}}\right)\left(1 - \frac{2z_c}{R_e}\right) - \frac{\alpha}{R_e}\left(\frac{2}{T_c} + \frac{1}{T_{c+1}} + \frac{3}{T_{c+2}}\right)\right]\beta^2 + \left[\frac{-6k}{g_0 m_a} \ln\left(\frac{P_{c+1}}{P_c}\right) + 2\alpha\left(\frac{1}{T_{c+1}} - \frac{1}{T_{c+2}}\right)\left(1 - \frac{2z_c}{R_e}\right) + \frac{\alpha^2}{R_e}\left(\frac{2}{T_c} + \frac{3}{T_{c+1}} + \frac{1}{T_{c+2}}\right)\right] \times \beta + \alpha \frac{6k}{g_0 m_a} \ln\left(\frac{P_{c+2}}{P_c}\right) + \alpha^2\left(\frac{1}{T_{c+2}} - \frac{1}{T_c}\right)\left(1 - \frac{2z_c}{R_e}\right) + \frac{\alpha^3}{R_e}\left(\frac{1}{T_{c+2}} - \frac{1}{T_c}\right) = 0. \quad (12)$$

The value for $\beta$ is taken as the smallest positive real root of Eq. (12).

One then proceeds downward, calculating $z_{c+3}$ from $z_{c+2}$ and $z_{c+1}$, $z_{c+4}$ from $z_{c+3}$ and $z_{c+2}$ and so on for tangent heights as low as 12 km. This approach gives an atmospheric model that obeys hydrostatic equilibrium by design. It also expresses tangent height as an analytical function of $P$ and $T$, permitting analytical calculation of the derivatives associated with least-squares fitting, thereby speeding up the retrieval process (compared with calculating derivatives numerically).

### 3. Pressure/Temperature Microwindows

The $CO_2$ microwindows used for ACE-FTS P/T retrievals are carefully selected to minimize interferences from other molecules, and so interferences are neglected in the fitting. Only the main isotopologue of $CO_2$ ($^{16}O^{12}C^{16}O$) is represented in the microwindows. Infrared absorption measurements are less susceptible to nonlocal thermodynamic equilibrium[26] (non-LTE) effects than IR emission measurements. Non-LTE effects induce a larger percentage change in the population of the initial state for emission than for absorption. However, vibrational non-LTE effects have been identified in thermospheric ATMOS spectra covering the $\nu_3$ band.[27] Thus the P/T microwindow set for ACE-FTS was restricted to a common lower-state vibration for altitudes greater than 70 km in order to minimize potential residual effects from non-LTE.

Microwindows were selected in the following wavenumber ranges: 932–937, 1890–1976, 2042–2073, 2277–2393, 2408–2448, 3301–3380, and 3570–3740 $cm^{-1}$.

### 4. Pressure and Temperature a priori

The first step in the P/T retrieval process is to generate a first guess for the pressure and the temperature profiles. From 150 km down to a few kilometers below the stratopause, $P$ and $T$ are calculated with the MSIS software. MSIS is primarily intended for application to the thermosphere and is unreliable at low altitudes. Thus *a priori* $P$ and $T$ below ~30 km is derived from meteorological data

from the Canadian Meteorological Centre (CMC). The Canadian operational weather analysis and forecast system at CMC-consists of the global environmental multiscale (GEM) model presented by Côté *et al.*[28,29] and a three-dimensional-var data assimilation system described by Gauthier *et al.*[30] and Laroche *et al.*[31] High-altitude profiles (from MSIS) and the corresponding low-altitude profiles (from the CMC) are spliced together by linear interpolations: linear in $T$ and in the natural logarithm of $P$.

It should be stressed that these pressure and temperature profiles are used only as first guesses. The fitting routine does not impose constraints based on *a priori* (i.e., we do not use an optimal estimation), and so the retrieval results are not sensitive to the first guess. The only altitude region where *a priori* information is crucial is below 12 km, where pressure and temperature are fixed to the meteorological data. The P/T retrievals would be unlikely to improve on the *a priori* information in this region, and so no attempt is made to do so. Note, however, that VMR retrievals extend to altitudes less than 12 km.

*5. First-Guess Tangent Heights*

As mentioned above, tangent heights at low altitudes (as high as 43 km) are calculated from the satellite ephemeris. First-guess tangent densities for measurements below ~25 km are calculated from Eq. (8) by using the following values for the coefficients: $a = 43.64$, $b = -42.07$, $c = 1.06$, and $d = -0.9357$. First-guess tangent heights for the measurements are then taken as altitudes corresponding to $\rho_{\text{tangent}}$ in the CMC data. These first-guess tangent heights are typically good to better than 0.5 km for tangent heights greater than 6 km. This is a very robust approach to the difficult challenge of obtaining initial estimates for tangent heights in this altitude region.

Between 25 and 43 km, refraction effects cause tangent heights to deviate from the geometric calculations, but Eq. (8) cannot be used because $R_b$ is equal to 1. (There is no significant continuum contribution to the spectrum.) In this altitude region, refraction effects on tangent heights do not vary widely from occultation to occultation, and so we use a crude empirical expression:

$$z_{\text{tangent}} \approx z_{\text{geom}} + 16.13 - 0.758 z_{\text{geom}} + 0.009016 z_{\text{geom}}^{2}, \tag{13}$$

where $z_{\text{geom}}$ is the tangent height calculated from the geometry. Expression (13) is not expected to be particularly accurate (sometimes it is in error by 1 or 2 km), but accurate first guesses are not required in the given altitude region.

*6. Low-Altitude Tangent Heights*

The ACE-FTS P/T retrievals occur on a relative altitude grid rather than an absolute altitude grid. The first-guess tangent heights described in Subsection 3.B.5 are not sufficiently accurate to provide a registration to absolute altitude. For measurements between 12 and 20 km, improved estimates of their tangent heights are determined by least-squares fitting with $P$ and $T$ fixed to CMC values. In this process, selected $CO_2$ lines are fitted with a single fitting parameter (tangent height) along with the usual baseline scale and slope parameters in each spectral window.

Table 2. $^{16}O^{12}C^{18}O$ Microwindows (Altitudes ≤ 25 km)

| Center ($cm^{-1}$) | Width ($cm^{-1}$) |
|---|---|
| 2611.30 | 0.35 |
| 2616.45 | 0.40 |
| 2620.84 | 0.50 |
| 2626.70 | 0.80 |
| 2636.63 | 0.30 |

This tangent-height determination is performed at the beginning of the retrieval process. The altitudes generated in this step are stored for eventual comparison with the altitudes determined during the P/T retrieval. At the end of the P/T retrieval, all tangent heights are shifted by a common amount to align the measurements between 12 and 20 km with the predetermined tangent heights. Note that this procedure would not be necessary if one trusted the high-altitude tangent heights calculated from geometry. It is errors in the ACE-FTS time stamp as well as the potential for an offset of the ACE-FTS field of view from the suntracker axis that necessitate this approach for altitude registration.

The $CO_2$ microwindows selected for this procedure are in Table 2. They consist of a set of weak $^{16}O^{12}C^{18}O$ lines near 2620 $cm^{-1}$. It is difficult to find quality $CO_2$ microwindows that extend to low altitude, but these $^{16}O^{12}C^{18}O$ microwindows extend as low as 5 km with little spectral interference. Unfortunately there appears to be an inconsistency in line intensities between these $^{16}O^{12}C^{18}O$ and $^{16}O^{12}C^{16}O$ lines. Fitted tangent heights between 12 and 20 km differ by ~350 m when lines from the two different isotopologues are used. This could be a result of systematic errors in the strengths of the $^{16}O^{12}C^{18}O$ lines in the line list and/or an actual physical difference in the VMRs from the expected $^{18}O/^{16}O$ isotopic ratio. To account for the discrepancy, the $CO_2$ VMR is increased by 3.5% whenever the $^{16}O^{12}C^{18}O$ microwindows in Table 2 are used. With this adjustment, discrepancies between fitted tangent heights in the 12–20 km range for the two isotopologues are reduced to less than ~100 m.

At the very end of the P/T retrieval process, after pressure, temperature, and tangent heights greater than 12 km have been finalized, the tangent heights for measurements less than 12 km (down to ~5 km) are determined by fitting the microwindows in Table 2, again simple by using tangent height as a fitting parameter with pressure and temperature fixed. Investigations are planned to determine whether the $N_2$ + $CO_2$ continuum can be used to establish low-altitude tangent heights rather than employing this simplistic fitting approach.

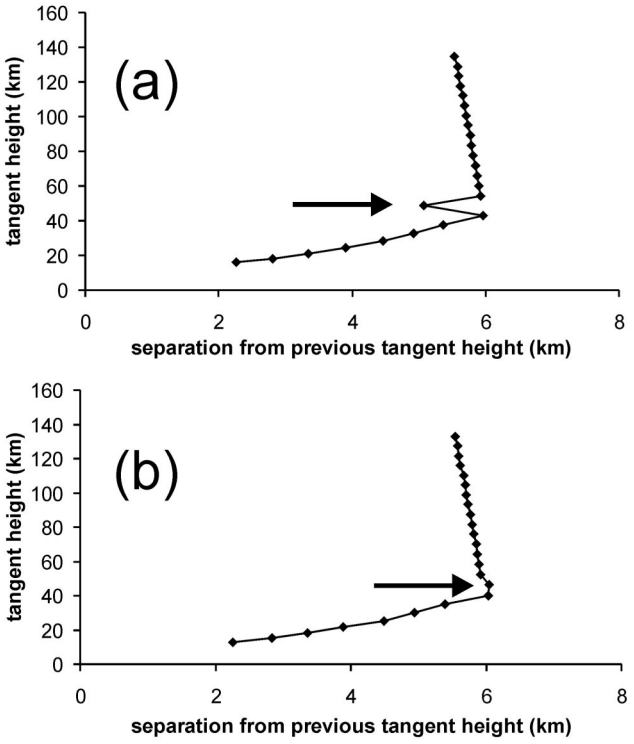


Fig. 4. Retrieved tangent heights for occultation sunset 3064 measured 7 March 2004, latitude 78.8° N, longitude 93.2°. (a) With the initial value determined for the pressure at the crossover measurement the first calculated tangent height during the low-altitude retrieval (indicated by the arrow) is out by more than 800 m. (b) After the refinement of the reference pressure the first retrieved tangent height (indicated by the arrow) is closer to expectations.

### 7. *Determining $P_c$*

Although the pressure at the crossover $P_c$ can be fitted, it is preferred that an accurate value for the parameter be determined and then fixed during the retrieval process. A first estimate is derived by performing the high-altitude retrieval depicted in Fig. 2 with $P_c$ as a fitting parameter. One then proceeds to the low-altitude retrieval depicted in Fig. 3 with $P_c$ fixed to the results of the high-altitude retrieval. If there is an error in $P_c$, there is a compensating error in the highest calculated tangent height and little effect below that. This is illustrated in Fig. 4 in which retrieved tangent-height separations are plotted in a manner to emphasize deviations from regular behavior. After the first pass at the retrieval [Fig. 4(a)] the highest calculated tangent height is clearly an outlier, a result of compensating for the error in $P_c$. The value of $P_c$ is then scaled to force the highest calculated tangent height to match expectations, leading to much smoother behavior [Fig. 4(b)] as one expects for a properly functioning suntracker.

The correction for $P_c$ is calculated from knowledge of the sensitivity of the highest calculated tangent height ($z_{c+2}$) to $P_c$. The derivatives of tangent height with respect to pressures are known, generated for the derivative calculations in the least-squares process. An improved value for the pressure at the crossover measurement is calculated as

$$P_c^{\text{new}} = P_c + \frac{\Delta z}{\dfrac{\mathrm{d}z_{c+2}}{\mathrm{d}P_{c+1}}\dfrac{P_{c+1}}{P_c} + \dfrac{\mathrm{d}z_{c+2}}{\mathrm{d}P_c}}, \tag{14}$$

where $\Delta z$ is the error in tangent height (the tangent height calculated from geometry minus the tangent height calculated in the first pass of the retrieval). Note that there is a term from the measurement below the crossover because its pressure $P_{c+1}$ is calculated from the crossover pressure. After the refined value for $P_c$ has been determined, both the high- and low-altitude retrievals are repeated with the parameter fixed.

### C. Volume Mixing Ratio Retrievals

Once atmospheric P and T profiles have been established, analysis proceeds to the VMR profiles of the atmospheric constituents. The fitting parameters are the VMRs at the tangent heights along with continuum (baseline scale and tilt) parameters. The VMR profile above the highest analyzed measurement is taken as a constant times the input guess profile.

The molecules retrieved on a routine basis for Version 1.0 were the following: $H_2O$, $O_3$, $N_2O$, CO, $CH_4$, NO, $NO_2$, $HNO_3$, HF, HCl, $ClONO_2$, $N_2O_5$, CFC-11, CFC-12, $COF_2$, HCFC-22, HDO, and $SF_6$. In Version 2.0 the following molecules were added to routine processing: HCN, $CH_3Cl$, $CF_4$, $C_2H_2$,$C_2H_6$, and $N_2$. HDO was removed from the processing to await a future version where other isotopologues were also retrieved. For Version 2.1 processing the retrievals of ClO were added. ClO normally has too low a concentration to retrieve, but the molecule can experience a dramatic increase in concentration from chemistry associated with polar stratospheric clouds.[32] In Version 2.2 the retrieval of the following weak absorbers was added: HOCl, $H_2O_2$, and $HO_2NO_2$. The retrieval of subsidiary isotopes also began with this version, including $^{13}CH_4$, $CH_3D$, $H_2{}^{18}O$, $H_2{}^{17}O$, and HDO, although there is a known problem with the HDO results that will be addressed in a future version.

$CCl_4$ will be included in the next version of ACE-FTS processing along with additional isotopologues. We also plan to retrieve CFC-113 and HCFC-142b, which have been seen from space for the first time by the ACE mission.[33]

As mentioned above, calculations employ the HITRAN 2004 line list. For heavy molecules with no line-by-line information (e.g., $N_2O_5$ and CFCs), cross-section data in HITRAN 2004 are interpolated to the appropriate pressure and temperature for a given altitude.

First-guess profiles for the VMR retrievals are taken from the results of the ATMOS missions. These profiles are perhaps outdated; but the ACE-FTS retrievals are not sensitive to *a priori* information except for the shape of the first-guess profile above the highest analyzed measurement.

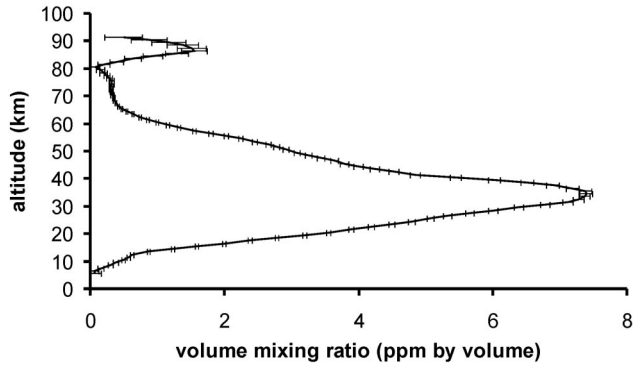


Fig. 5. Retrieved ozone profile for the occultation sunset 8430 measured 7 March 2005, latitude 79.8° N, longitude 133° W. Error bars are the 1σ statistical fitting errors and do not include systematic contributions to the uncertainty.

Each molecule is analyzed separately. The microwindows selected for a given molecule may contain significant spectral interference from other molecules (particularly for molecules with broad absorption features such as $N_2O_5$). A multiple molecule fitting approach is employed to simultaneously retrieve VMR profiles for the molecule of interest and significant interferers. The retrieval results for the interferers are discarded.

Figure 5 shows the retrieval results from March 2005 for $O_3$. Ozone retrievals for Version 1.0 of the ACE-FTS processing software extended only as high as 70 km. However, the excellent SNR of the instrument permits us to see absorption features to a much higher altitude. In Version 2.0 and higher the retrieval range is therefore extended to altitudes higher than 90 km. As can be seen in Fig. 5 this gives valuable information on the secondary peak of ozone at high altitudes.

The winter/spring of 2004 saw a dramatic increase in $NO_x$ in the Arctic region.[34,35] Figure 6 shows the retrieved profiles for NO and $NO_2$ from February 2004. Both molecules exhibit a significant spike in the VMR at the same altitude. This can be attributed to NO created at high altitudes and transported downward. More details on the phenomenon can be found in the paper by Rinsland *et al.*[35]

Figure 7 shows VMR retrieval results from June 2004 for HCl and HF. HCl and HF are key species in the atmospheric halogen budget, and the ACE-FTS and HALOE instruments are currently the only satellite instruments that can measure both molecules. Comparisons of HCl and HF with results from HALOE indicate significant discrepancies[36] (~15%) with similar percentage differences for the two molecules. This matter is still being investigated, but preliminary comparisons with results for HCl from the Microwave Limb Sounder instrument on the Aura satellite show good agreement with ACE-FTS results.[37]

## 4. Retrieval Errors

The uncertainties reported for the ACE-FTS results are the statistical fitting errors from the least-

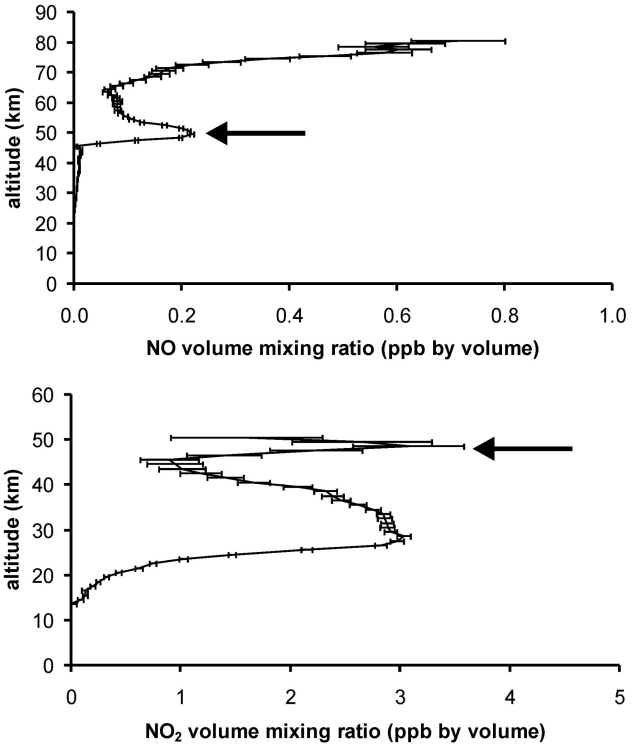


Fig. 6. NO (upper panel) and $NO_2$ (lower panel) profiles for sunset 2806 measured 19 February 2004, latitude 74° N, longitude 72° E. Arrows indicate unusual, coincident peaks in the two profiles near 50 km. Error bars are the 1σ statistical fitting errors.

squares process, assuming a normal distribution of random errors. As of Version 2.2 neither systematic contributions nor parameter correlations are accounted for in the reported uncertainties. A later analysis incorporates systematic contributions to errors, such as carrying forward errors in the P/T retrievals to the VMR retrievals.

Recent work has been done by ACE science team members in Belgium to develop VMR retrieval software based on the optimal estimation approach.[38] A more detailed error budget was determined for CO retrievals,[39] including systematic contributions from P/T retrievals and uncertainties in the empirical ILS parameters in Eq. (3). These errors were found to be comparable with the statistical errors from our retrievals. This study will be expanded to other molecules and to P/T retrievals to get a better sense of the errors inherent in the ACE-FTS retrieval results and to provide a measure of software validation.

## 5. Processing Details

Routine ACE-FTS processing takes place on a small cluster of Sun Fire compute nodes. The cluster comprises 16 64-bit processors (operating at 1.3 GHz) and 20 GB total memory. The nodes are interconnected with a private 100 Mbps network and have direct access to other ACE computer systems. The ACE database server is a four-processor Sun Fire 3800 with 5 TB of storage. To maximize the throughput of the cluster, all levels of data processing are

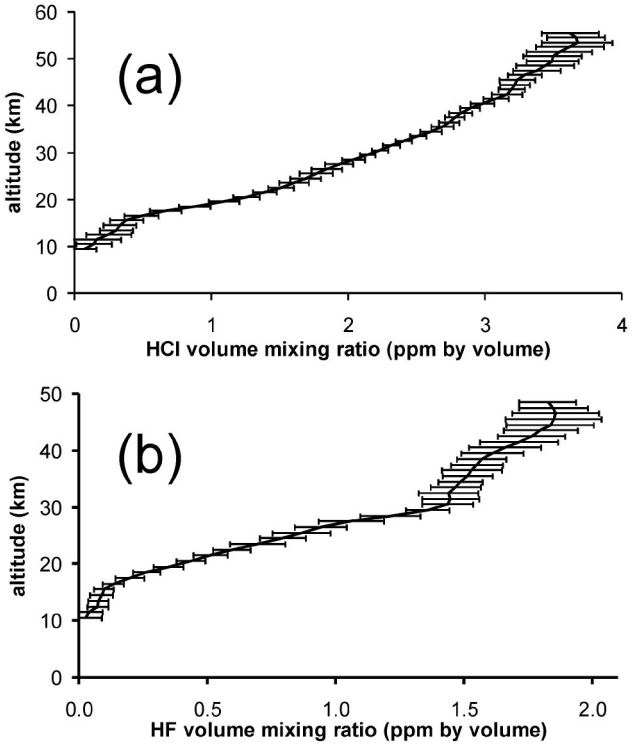


Fig. 7. Average VMR profiles for 20 occultations measured from 27 June 2004 through 30 June 2004 with latitudes 44–54° N. Error bars are the standard deviation of the averaged profiles and do not account for fitting uncertainties: (a) Average profile for HCl; (b) average profile for HF.

managed by the OpenPBS job queuing system, which keeps each node working continuously. All data for the mission are organized in databases by using the open source PostgreSQL software.

Because of the nature of solar occultation, ACE has a relatively low rate of measurement opportunities, on average 30 occultations per calendar day. As a scientific research mission there is no requirement for near-real-time processing, but it is important for processing to occur in a timely fashion to avoid falling behind, particularly if one wants to reanalyze all the data for a new version. The ACE-FTS software uses all analytical derivative calculations (rather than numerical) for improved speed. All necessary data are stored in temporary arrays to avoid the need for continuous read/write operations. This makes for a large memory footprint for the software (3–3.5 Gbytes).

For additional analysis speedups the matrix inversion in the least-squares process exploits the sparse nature of the matrices involved. For VMR retrievals the derivatives of the calculated signal with respect to the parameters are calculated explicitly for the first two iterations in the least-squares fitting; thereafter the derivatives are simply reused (as long as $\chi^2$ is not too large). Note that the derivatives for P/T retrievals cannot be recycled in this fashion because they exhibit greater variability.

The processing time for a single occultation (a P/T retrieval followed by VMR retrievals for 23 or 24 molecules) typically takes 3–5 h on one of the Sun Fire nodes. Because the rate of data collection is on average 1 occultation every 90 min, processing is performed in parallel on the 16 nodes. This allows the processing to keep pace with the influx of new data with a margin available to permit reprocessing of the data set with new software versions.

## 6. Discussion and Results

A flow chart summarizing the P/T retrieval process is presented in Fig. 8. The VMR retrieval process is much simpler, simply taking as inputs the pressure, temperature, and tangent-height information determined during the P/T retrieval.

Figure 9 illustrates an example of problems experienced with Version 1.0 when there were multiple measurements within a single 1 km layer. There is a large spike near 17 km for the profile in Fig. 9(a), retrieved with Version 1.0 of the processing software, but the spike does not appear when the profile is retrieved with Version 2.1 [Fig. 9(b)]. This is an extreme example, the magnitudes of spikes in the retrieved temperature profile were not typically that large (and in fact did not always occur for this situation). No such spikes occur for Version 2.0 or higher. There is also a less obvious spike at the mesopause in Fig. 9(a), diagnosed by an accompanying spike in the retrieved $CO_2$ VMR profile (not shown) for the occul-

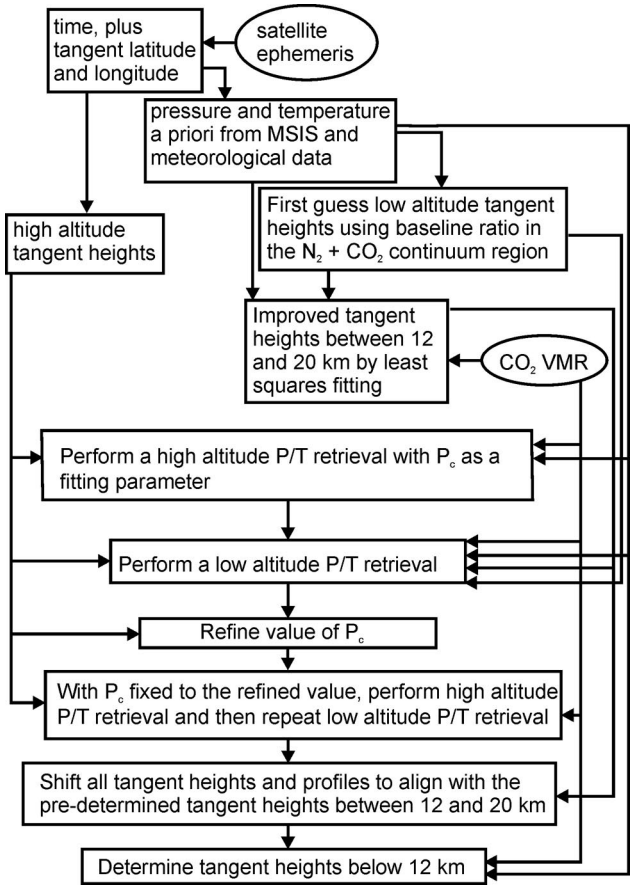


Fig. 8. Flowchart describing the P/T retrieval process.

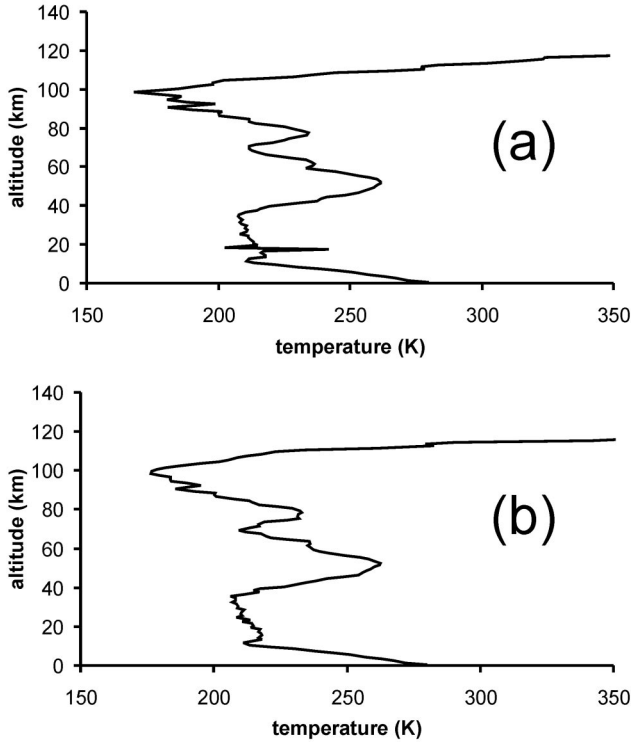


Fig. 9. Retrieved temperature profile for sunset 2727 measured 14 February 2004, latitude 57.3° N, longitude 133.4° W: (a) retrieval with Version 1.0 of the ACE-FTS processing software, (b) retrieval with Version 2.1.

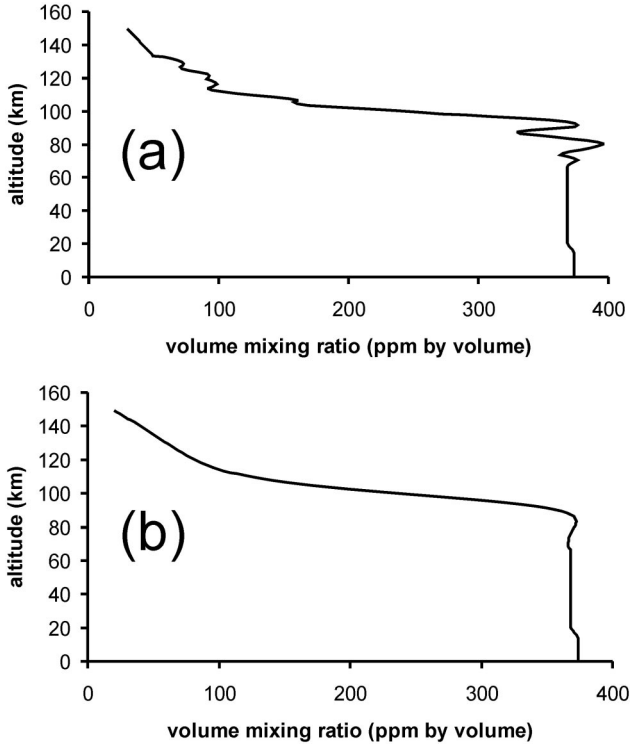


Fig. 10. $CO_2$ VMR profile from the P/T retrieval for the occultation sunrise 4326 measured 1 June 2004, latitude 49° N, longitude 93° W. The VMR profile is fixed below 70 km and retrieved above: (a) retrieval with Version 2.0 of the processing software; (b) retrieval with Version 2.1.

tation. Figure 9(b) features improved results in this altitude region due to the empirical expression used for high-altitude $CO_2$ VMR.

A comparison of $CO_2$ VMR profiles for Versions 2.0 and 2.1 is shown in Fig. 10. The portion of the profile below ~70 km is fixed, while the portion above is retrieved. For Version 2.0 this occultation showed ~10% variability in retrieved $CO_2$ between 80 and 90 km. Recall that Version 2.0 retrieves $CO_2$ VMR at each tangent height greater than 70 km, while Version 2.1 retrieves the parameters in an empirical function [Eq. (7)]. Also Version 2.1 uses more points in the ILS for this altitude region, which better accounts for far wing contributions in the microwindows. The profile retrieved with Version 2.1 removed most of the (presumably unphysical) variability.

Validation efforts for the temperature retrievals are in progress. Correlative comparisons with independent data (National Centers for Environmental Prediction, European Centre for Medium-Range Weather Forecasts, radiosondes) typically show good (within 3–5 K) agreement.[1] Figure 11 presents a comparison of retrieved temperature (Version 2.0) from the ACE-FTS with measurements taken by a radiosonde launched from the Eureka weather station. The agreement is within 3 K, typically better than 1–2 K. The radiosonde measures small-scale structure that the ACE-FTS cannot resolve because of its coarser altitude sampling. It should be emphasized again that *a priori* information is not used as a constraint in the fitting. Sensitivity studies indicate that ACE-FTS retrieved temperatures are consistent to within 1 K even for dramatically different initial guess profiles.

Validation of the VMR retrieval results is also ongoing. Preliminary studies with Version 1.0 show promise but also a few issues that require further investigation, such as the bias mentioned above for HALOE HCl and HF and a 5–10% low bias at the

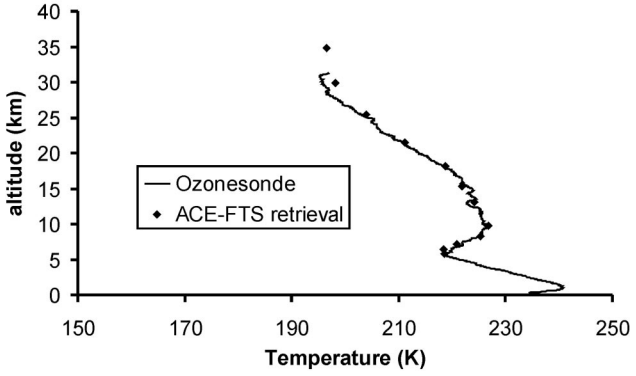


Fig. 11. Temperature retrieval results for sunset 3064, measured 7 March 2004, latitude 78.8° N, longitude 93.2° W. Comparison is made with measurements taken by a radiosonde launched from the Eureka weather station (latitude 80° N, longitude 85.8° W). The radiosonde launch differed from the ACE occultation by 33 min in time and 202.5 km in distance.

ozone concentration peak compared with some visible spectrometers.[40]

We thank Marty McHugh for providing the HALOE $CO_2$ equation and Manuel Lopez-Puertas for providing a comparison $CO_2$ profile. Funding was provided by the Canadian Space Agency and the Natural Sciences and Engineering Research Council (NSERC) of Canada as well as the NSERC–Bomem–Canadian Space Agency–Meteorological Service of Canada Industrial Research Chair in Fourier-transform spectroscopy.

## References

1. P. F. Bernath, C. T. McElroy, M. C. Abrams, C. D. Boone, M. Butler, C. Camy-Peyret, M. Carleer, C. Clerbaux, P.-F. Coheur, R. Colin, P. DeCola, M. De Mazière, J. R. Drummond, D. Dufour, W. F. J. Evans, H. Fast, D. Fussen, K. Gilbert, D. E. Jennings, E. J. Llewellyn, R. P. Lowe, E. Mahieu, J. C. McConnell, M. McHugh, S. D. McLeod, R. Michaud, C. Midwinter, R. Nassar, F. Nichitiu, C. Nowlan, C. P. Rinsland, Y. J. Rochon, N. Rowlands, K. Semeniuk, P. Simon, R. Skelton, J. J. Sloan, M.-A. Soucy, K. Strong, P. Tremblay, D. Turnbull, K. A. Walker, I. Walkty, D. A. Wardle, V. Wehrle, R. Zander, and J. Zou, "Atmospheric Chemistry Experiment (ACE): mission overview," Geophys. Res. Lett. **32,** L15S01, doi:10.1029/2005GL022386 (2005).
2. M. R. Gunson, M. M. Abbas, M. C. Abrams, M. Allen, L. R. Brown, T. L. Brown, A. Y. Chang, A. Goldman, F. W. Irion, L. L. Lowes, E. Mahieu, G. L. Manney, H. A. Michelsen, M. J. Newchurch, C. P. Rinsland, R. J. Salawitch, G. P. Stiller, G. C. Toon, Y. L. Yung, and R. Zander, "The Atmospheric Trace Molecule Spectroscopy (ATMOS) experiment: Deployment on the ATLAS Space Shuttle missions," Geophys. Res. Lett. **23,** 2333–2336 (1996).
3. R. Beer, T. A. Glavich, and D. M. Rider, "Tropospheric emission spectrometer for the Earth Observing System's Aura satellite," Appl. Opt. **40,** 2356–2367 (2001).
4. H. Fischer and H. Oelhaf, "Remote sensing of vertical profiles of atmospheric trace constituents with MIPAS limb-emission spectrometers," Appl. Opt. **35,** 2787–2796 (1996).
5. W. P. Chu, M. P. McCormick, J. Lenoble, C. Brogniez, and P. Pruvost, "SAGE II inversion algorithm," J. Geophys. Res. **94,** D6, 8339–8352 (1989).
6. M.-A. Soucy, F. Chateauneuf, H. Buijs, C. Deutsch, S. Fortin, R. Poulin, N. Etienne, G. Paquet, P. Bernath, K. Walker, P. Tremblay, J. Drummond, D. Turbull, and K. Gilbert, "ACE-FTS instrument design and on-orbit status," Appl. Opt. (to be published).
7. M. N. Eremenko, A. Y. Zasetsky, C. D. Boone, and J. J. Sloan, "Properties of high-altitude tropical cirrus clouds determined from ACE FTS observations," Geophys. Res. Lett. **32,** L15S07, doi:10.1029/2005GL022428 (2005).
8. G. P. Stiller, M. R. Gunson, L. L. Lowes, M. C. Abrams, O. F. Raper, C. B. Farmer, R. Zander, and C. P. Rinsland, "Stratospheric and mesospheric pressure-temperature profiles from rotational analysis of $CO_2$ lines in atmospheric trace molecule spectroscopy/ATLAS 1 infrared solar occultation spectra," J. Geophys. Res. **100,** 3107–3117 (1995).
9. T. von Clarmann, N. Glatthor, U. Grabowski, M. Höpfner, S. Kellerman, M. Kiefer, A. Linden, G. M. Tsidu, M. Milz, T. Steck, G. P. Stiller, D. Y. Wang, and H. Fischer, "Retrieval of temperature and tangent altitude pointing from limb emission spectra recorded from space by the Michelson interferometer for passive atmospheric sounding (MIPAS)," J. Geophys. Res. **108,** 4736–4750 (2003).
10. M. Carlotti, "Global-fit approach to the analysis of limb-scanning atmospheric measurements," Appl. Opt. **27,** 3250–3254 (1988).
11. W. H. Press, B. P. Flannery, S. A. Teukolsky, and W. T. Vetterling, *Numerical Recipes in Fortran,* 2nd ed. (Cambridge University, 1992).
12. *WGS 84 Implementation Manual Version 2.4* (European Organization for the Safety of Air Navigation, Brussels, Belgium, the Institute of Geodesy and Navigation, University FAF, Munich, Germany, 1998).
13. M. López-Puertas, M. A. López-Valverde, R. R. Garcia, and R. G. Roble, "A review of $CO_2$ and CO abundances in the middle atmosphere," Atmospheric Science across the Stratopause, Geophysical Monograph 123 (American Geophysical Union, 2000), pp. 83–100.
14. R. G. Roble, "On the feasibility of developing a global atmospheric model extending from the ground to the exosphere," Atmospheric Science Across the Stratopause, Geophysical Monograph 123 (American Geophysical Union, 2000), pp. 53–67.
15. J. M. Russell III, L. L. Gordley, J. H. Park, S. R. Drayson, D. H. Hesketh, R. J. Cicerone, A. F. Tuck, J. E. Frederick, J. E. Harries, and P. J. Crutzen, "The Halogen Occultation Experiment," J. Geophys. Res. **98,** 10,777–10,797 (1993).
16. L. S. Rothman, D. Jacquemart, A. Barbe, D. C. Benner, M. Birk, L. R. Brown, M. R. Carleer, C. Chackerian Jr, K. Chance, L. H. Coudert, V. Dana, V. M. Devi, J.-M. Flaud, R. R. Gamache, A. Goldman, J.-M. Hartmann, K. W. Jucks, A. G. Maki, J.-Y. Mandin, S. T. Massie, J. Orphal, A. Perrin, C. P. Rinsland, M. A. H. Smith, J. Tennyson, R. N. Tolchenov, R. A. Toth, J. Vander Auwera, P. Varanasi, and G. Wagner, "The HITRAN 2004 molecular spectroscopic database," J. Quant. Spectrosc. Radiat. Transfer **96,** 139–204 (2005).
17. J. Fischer, R. R. Gamache, A. Goldman, L. S. Rothman, and A. Perrin, "Total internal partition sums in the 2000 edition of the HITRAN database," J. Quant. Spectrosc. Radiat. Transfer **82,** 401–412 (2003).
18. M. Kuntz, "A new implementation of the Humlicek algorithm for the calculation of the Voigt profile function," J. Quant. Spectrosc. Radiat. Transfer **57,** 819–824 (1997).
19. M. Kuntz, "A new calculation of the Humlicek algorithm for the calculation of the Voigt profile function," **57,** 819–824 (1997); W. Ruyten, "A new implementation of the Humlicek algorithm for the calculation of the Voigt profile function: comment," J. Quant. Spectrosc. Radiat. Transfer **86,** 231–233 (2004).
20. S. P. Davis, M. C. Abrams, and J. W. Brault, *Fourier Transform Spectroscopy* (Academic, 2001).
21. R. H. Norton and R. Beer, "New apodizing functions for Fourier spectrometry," J. Opt. Soc. Am. **66,** 259–264 (1976); erratum, **67,** 419 (1977).
22. C. D. Boone, S. D. Mcleod, and P. F. Bernath, "Apodization effects in the retrieval of volume mixing ratio profiles," Appl. Opt. **41,** 1029–1034 (2002).
23. U. Amato, D. de Canditiis, and C. Serio, "Effect of apodization on the retrieval of geophysical parameters from Fourier-transform spectrometers," Appl. Opt. **37,** 6537–6543 (1998).
24. J. M. Picone, A. E. Hedin, D. P. Drob, and A. C. Aikin. "NRLMSISE-00 empirical model of the atmosphere: statistical comparisons and scientific issues," J. Geophys. Res. **107** (A12), 1468–1483 (2002).
25. C. P. Rinsland, M. J. McHugh, and F. W. Irion, "Lower stratospheric densities from solar occultation measurements of continuum absorption near 2400 $cm^{-1}$," J. Geophys. Res. **109** (D1), 1301–1308 (2004).
26. C. J. Mertens, M. G. Mlynczak, M. López-Puertas, P. P. Wintersteiner, R. H. Picard, J. R. Winick, L. L. Gordley, and J. M. Russell III, "Retrieval of mesospheric and lower thermospheric kinetic temperature from measurements of $CO_2$ 15 μm

Earth limb emission under non-LTE conditions," Geophys. Res. Lett. **28,** 1391–1394 (2001).
27. C. P. Rinsland, M. R. Gunson, R. Zander, and M. López-Puertas, "Middle and upper atmosphere pressure-temperature profiles and the abundances of $CO_2$ and CO in the upper atmosphere from ATMOS/Spacelab 3 observations," J. Geophys. Res. **97,** 20,479–20,495 (1992).
28. J. S. Côté, S. Gravel, A. Méthot, A. Patoine, M. Roch, and A. Staniforth, "The operational CMC-MRB global environmental multiscale (GEM) model. Part I: Design considerations and formulations," Mon. Weather Rev. **126,** 1373–1395 (1998).
29. J. Côté, J.-G. Desmarais, S. Gravel, A. Méthot, A. Patoine, M. Roch, and A. Staniforth, "The operational CMC-MRB global environmental multiscale (GEM) model. Part II: Results," Mon. Weather Rev. **126,** 1397–1418 (1998).
30. P. C. Gauthier, C. Charette, L. Fillion, P. Koclas, and S. Laroche, "Implementation of a 3D variational data assimilation system at the Canadian Meteorological Centre. Part I: The global analysis," Atmos. Ocean **37,** 103–156 (1999).
31. S. Laroche, P. Gauthier, J. St-James, and J. Morneau, "Implementation of a 3D variational data assimilation system at the Canadian Meteorological Centre. Part II: The regional analysis," Atmos. Ocean **37,** 281–307 (1999).
32. N. Glatthor, T. von Clarmann, H. Fischer, U Grabowski, M. Hopfner, S. Kellmann, M. Kiefer, A. Linden, M. Milz, T. Steck, G. P. Stiller, G. M. Tsidu, and D.-Y. Wang, "Spaceborne CIO observations by the Michelson Interferometer for Passive Atmospheric Sounding (MIPAS) before and during the Antarctic major warming in September/October 2002," J. Geophys. Res. **109,** D11,307–11,317 (2004).
33. G. Dufour, C. D. Boone, and P. F. Bemath, "First measurements of CFC-113 and HCFC-142b from space using ACE-FTS infrared spectra," Geophys. Res. Lett. **32,** L15S09, doi: 10.1029/2005GL022422 (2005).
34. C. E. Randall, V. L. Harvey, G. L. Manney, Y. Orsolini, M. Codrescu, C. Sioris, S. Brohede, C. S. Haley, L. L. Gordley, J. M. Zawodny, and J. M. Russell III, "Stratospheric effects of energetic particle precipitation in 2003–2004," Geophys. Res. Lett. **32,** L05802–L05805 (2005).
35. C. P. Rinsland, P. F. Bernath, C. D. Boone, R. Nassar, K. A. Walker, J. C. McConnell, and L. Chiou, "Atmospheric Chemistry Experiment (ACE) Arctic stratospheric measurements of $NO_x$ and long-lived tracers during February and March 2004: impact of intense solar flares," Geophys. Res. Lett. **32,** L16S05, doi:10.1029/2005GL022425 (2005).
36. M. McHugh, B. McGill, K. A. Walker, C. D. Boone, P. F. Bernath, and J. M. Russell III, "Comparison of atmospheric retrievals from ACE and HALOE," Geophys. Res. Lett. **32,** L15S08, doi:10.1029/2005GL022396 (2005).
37. L. Froidevaux, N. J. Livesey, W. G. Read, Y. B. Jiang, C. C. Jimenez, M. J. Filipiak, M. J. Schwartz, M. L. Santee, H. C. Pumphrey, J. H. Jiang, D. L. Wu, G. L. Manney, B. J. Drouin, J. W. Waters, E. J. Fetzer, P. F. Bernath, C. D. Boone, K. A. Walker, K. W. Jucks, G. C. Toon, J. J. Margitan, B. Sen, C. R. Webster, L. E. Christensen, J. W. Elkins, E. Atlas, R. A. Lueb, and R. Hendershot, "Early validation analyses of atmospheric profiles from EOS MLS on the Aura satellite," submitted to IEEE Trans. Geosci. Remote Sensing (to be published).
38. C. D. Rodgers, *Inverse Methods for Atmospheric Sounding: Theory and Practice,* in Atmospheric Oceanic Planetary Physics, Series, Vol. 2, F. W. Taylor, ed. (World Scientific, 2000).
39. C. Clerbaux, P.-F. Coheur, D. Hurtmans, B. Barret, M. Carleer, R. Colin, K. Semeniuk, J. C. McConnell, C. D. Boone, and P. F. Bernath, "Carbon monoxide distribution from the ACE-FTS solar occultation measurements," Geophys. Res. Lett. **32,** L16S01, doi:10.1029/2005GL022394 (2005).
40. K. A. Walker, C. E. Randall, C. R. Trepte, C. D. Boone, and P. F. Bernath, "Initial validation comparisons for the Atmospheric Chemistry Experiment (ACE)," Geophys. Res. Lett. **32,** L16S04, doi:10.1029/2005GL022388 (2005).